Detection of seizure onset in childhood absence epilepsy

M Aud'Hui, A Kachenoura, Maxime Yochum, Anna Kamińska, Rima Nabbout, Fabrice Wendling, Mathieu Kuchenbuch, P Benquet

Detection of seizure onset in childhood absence epilepsy

Aud'hui M[1], Kachenoura A[1], Yochum M[1,c], Kaminska A[2], Nabbout R[2,3], Wendling F[1], Kuchenbuch M[4,a], Benquet P[1,a]

[a] *equal contribution*
[c] *corresponding author (maxime.yochum@univ-rennes.fr)*

[1] *Univ Rennes, INSERM, LTSI – UMR 1099, Rennes F-35000, France*

[2] *Department of Clinical Neurophysiology, Hôpital Necker Enfants Malades, AP-HP, Université de Paris, Paris, France.*

[3] *Reference Center for Rare Epilepsies, Department of Pediatric Neurology, Member of EPICARE Network, Institute Imagine INSERM 1163, Université de Paris, Paris, France.*

[4] *Pediatric and Genetic Department, CHU, Nancy, France*

Abstract

Objective: This study aims to detect the seizure onset, in childhood absence epilepsy, as early as possible. Indeed, interfering with absence seizures with sensory simulation has been shown to be possible on the condition that the stimulation occurs soon enough after the seizure onset.

Methods: We present four variations (two supervised, two unsupervised) of an algorithm designed to detect the onset of absence seizures from 4 scalp electrodes, and compare their performance with that of a state-of-the-art algorithm. We exploit the characteristic shape of spike-wave discharges to detect the seizure onset. Their performance is assessed on clinical electroencephalograms from 63 patients with confirmed childhood absence epilepsy.

Results: The proposed approaches succeed in early detection of the seizure onset, contrary to the classical detection algorithm. Indeed, the results clearly show the superiority of the proposed methods for small delays of detection, under 750 ms from the onset.

Conclusion: The performance of the proposed unsupervised methods is equivalent to that of the supervised ones. The use of only four electrodes makes the pipeline suitable to be embedded in a wearable device.

Significance: The proposed pipelines perform early detection of absence seizures, which constitutes a prerequisite for a closed-loop system.

Keywords

Childhood absence epilepsy; Scalp EEG; Seizure onset detection; Early detection; Spike-wave discharge; Dynamic time warping

Abbreviations

CAE, childhood absence epilepsy
GAERS, genetic absence epilepsy rat from Strasbourg
EEG, electroencephalogram
SWD, spike-wave discharge
EOI, event of interest
DTW, dynamic time warping
MLP, multilayer perceptron
Se, sensitivity
Pr, precision
FD/H, false detections per hour
SVM, support vector machine

1. Introduction

Absence seizures in Childhood Absence Epilepsy (CAE) are defined by a sudden complete and often relatively brief (<10 sec) loss of consciousness sometimes associated with automatisms or eyelid or perioral myoclonus (Panayiotopoulos, 1999) concomitant to regular 2.5-4 Hz generalized spike-waves. This type of seizure constitutes the main feature of CAE. Absence seizures are very distressing since they can occur very frequently, up to 200 per day (Crunelli and Leresche, 2002). This causes repeated disturbance of attention, working memory, information gating and finally transient disruption of learning that may lead to cognitive impairments (Fonseca Wald et al., 2019). Only 65% of children do outgrow their seizures and are able to stop taking medication (Wirrell et al., 1996). In addition, 18-35 % of children with absence seizures are pharmaco-resistant (Rinaldi et al., 2021).

Recent studies have shown that a cortical focal onset triggers the abrupt activation and sustained activity of the cortico-basal ganglia-thalamo-cortical loops and affects the normal physiological function of several cortical areas including the prefrontal

cortex, precuneus, posterior cingulate cortex, lateral parietal cortex among others (Crunelli et al., 2020).

In the Genetic Absence Epilepsy Rat from Strasbourg (GAERS) model, sensory stimulations have been shown to reduce seizures occurrence (Saillet et al., 2013). Some studies in human patients have shown that external stimulation, particularly loud or painful stimuli, can stop absence seizures (Blumenfeld, 2005). Based on the assessment of verbal response to questions and motor tests, individuals experiencing absence seizures generally exhibit minimal impairment during the initial 1–3 seconds and final 3–5 seconds but they do enter a phase of loss of consciousness (Blumenfeld, 2005). These observations suggest that the underlying subcortical-cortical loop that leads to seizures take only a few seconds to be fully installed. Indeed, one study has shown that acoustic stimuli applied at the onset was able to inhibit absence seizure and that the most effective inhibition was obtained if stimulation was applied during the first 3 s (Rajna and Lona, 1989).

However, once installed, the rhythmic activity of the cortico-subcortical loops cannot be stopped by an external somatosensory, auditory or visual stimulation. Therefore, the development of a method able to detect absence seizures within the shortest delays after their initiation could be of major importance. Some trials based on closed-loop stimulation have been performed in rat (Saillet et al., 2009; Maksimenko et al., 2017) and in computational modeling studies (Fan and Wang, 2020; Ge et al., 2019), but to date no efficient closed-loop system exist in clinic, in part because no signal processing algorithm has yet been designed for early seizure onset detection based on human scalp ElectroEncephaloGram (EEG), although a number of studies have been devoted to the automated detection of Spike-Wave Discharges (SWDs) in rodent models (van Luijtelaar et al., 2016) and in humans (Duun-Henriksen et al., 2012; Glaba et al., 2021; Kjaer et al., 2017; Swinnen et al., 2021).

In this study, we present four variations of an algorithm designed to detect the onset of absence seizures from two channel derivations (4 electrodes, a number of electrodes well suited for a portable device). We then compare their performance, not only in terms of accuracy but also in terms of latency, with those of a state-of-the-art SWD algorithms (Kjaer et al., 2017). Unlike most SWD algorithms, our pipelines do not rely on the spectral characteristics of the signal or one of its transforms to detect seizures, but on spike-wave detection modules, thus exploiting the characteristic signal shape of SWDs to detect the seizure from one or two spike-waves occurring at the onset. Of these two spike-wave detection modules, one, a MultiLayer Perceptron (MLP) classifier, is supervised, while the other one is unsupervised and based on the similarity with a template, computed with a variant of Dynamic Time Warping (DTW). Depending on the spike-wave detection module and on the number of consecutive spike-waves needed to mark a seizure, we have consequently four different pipelines.

2. Material and methods

2.1. Study design

This is a retrospective multicenter study conducted on children with CAE who had video-EEG recordings recorded from august 2013 to 2019 at two French hospital centers (Saint-Brieuc and Necker-Enfants malades). The study focused on children who experienced seizure onset at the age of 4 to 11 years and in whom video-EEG features are characteristic of CAE: on the one hand, electro clinical typical absence seizures, and on the other hand, a normal EEG background sometimes associated with occipital intermittent rhythmic delta activity, or interictal focal spikes or very short generalized SWDs. According to the new classification of syndromes, we followed exclusion criteria for this epileptic syndrome in particular: intellectual disability and potentially relevant neurological or neuroimaging abnormalities. This study followed the principles of declaration of Helsinki for human subject protection. Local ethics committees approved the study protocol (Agreement IRB N° IORG0010044, NCK-2020-R-050 PREDILEPSIE). According to the French MR-004 methodology, an information letter was sent to the legal representatives of each child included in the study and in absence of objection to the use of their retrospective data for clinical research, the EEG recordings were included in the database for processing.

2.2. EEG recordings

EEG recording respected the French recommendation for EEG in children (André-Obadia et al., 2015). EEGs were performed according to the 10/20 international system using 19 electrodes with Fpz as reference. Signals were amplified (1000 times), filtered at 0.1 to 120 Hz and acquired at 256 Hz using the Deltamed Natus (San Carlo, USA). In addition, a notch filter at 50 Hz is applied on all EEGs. The average duration of the EEG recording session was at least 20 minutes, with classical activation procedures (at least one intermittent photic stimulation and one 3-minute period of hyperventilation).

Seizure-free EEGs were discarded, as well as a small portion of EEGs showing atypical activity. 83 EEGs from 63 children were used to assess the performance of our algorithms (25 from Necker-Enfants Malades hospital and 38 from Saint-Brieuc hospital, 35 females and 28 males). Three separate ones were used for the training of the supervised methods. The average age at EEG-video recordings was 7.1 years. At this time, 19 children (30.2%) were not taking any antiseizure medication. Among those who were on medication, 17 were taking valproate (27%), 14 ethosuximide (22.2%), 4 lamotrigine (6.3%), and 9 were treated with a combination of antiseizure medications (14.3%). EEG recordings used in this study lasted a median 30 [24-43] minutes allowing the record of 4 [2-8] seizures per EEG. In total, we included 2694 minutes of EEG recordings counting 449 typical absence seizure.

2.3. Early seizure detection

Seizures were defined as trains of four or more spike-waves, clearly visible on most channels in a monopolar montage. This limit of four spike-waves was fixed following the clinicians' suggestions and its function is to discount isolated spike-waves or very short trains of spike-waves, which are less likely to be clinically symptomatic. Their onsets were manually labeled by 3 experts using conventional clinical scalp EEG with a transverse montage as illustrated in Fig. 1 A. The peak of the first spike-wave presents bilaterally on 4 or more channels was considered as the seizure onset. Note that, due to the presence of intra- and inter-individual variability, we did not label as the seizure onset the slow deviation which is often observed in the frontal channels preceding the SWD.

In order to anticipate an implementation in a wearable closed-loop system in child, only 4 channels were used. As illustrated in Fig. 1 B, the channel derivations Fp1-T3 and Fp2-T4, showing a high signal to noise ratio with prominent SWDs were used for automatic detection as in (Glaba et al., 2021).

Our algorithm operates using a sliding window approach. The first phase of the method involves determining if the window contains a spike-wave through confidence indexes. To accurately identify the onset of a seizure with the shortest possible delay, we employ a methodology that relies on the detection of a spike and half of a wave. At each time step (one sample), the algorithm progresses through three consecutive stages. The first two stages of this phase act as window selection filters and conclude with a decision on the presence of an Event Of Interest (EOI). If no EOI is detected, the algorithm proceeds to the next time step. Then, the third stage is a classification stage, where the current EOI window signal and its derivative are analyzed using one of two different classification methods: MLP or similarity to a template using DTW. This classification step determines whether the current window contains a spike-wave, based on a confidence index ranging from 0 to 1. Finally, the second phase involves a decision-making process that considers the probability of presence of one spike-wave or two consecutive spike-waves on two channels to detect the onset of a seizure. The procedure for early seizure detection is depicted in Fig 2 A, and signal examples are shown in Fig 2 A-B.

2.3.1. Spike wave Detection

2.3.1.1. Framing stage

Our approach uses a sliding window with a duration of 200 ms (number s of samples = 50), approximately matching the length of a spike and half a wave. The time step of the sliding window is one sample, ensuring that the entire signal is thoroughly examined. The framing stage is designed to retain windows that may encompass a "well-framed" spike-wave pattern. Specifically, the spike must be precisely located within the first half (from 0 to 100 ms) of the window, while the first half of the wave must be located in the second half of the window (from 100 ms to 200 ms).

To evaluate this, the algorithm searches for the maximum or minimum value of the derivative of the signal within the first half of the window. To ensure consistent timing of all spikes within the window, we have specified that the minimum or maximum must be precisely located at the framing point, which is at 1/3rd of the window (sample s1). If this condition is not met, no further detection is performed, and the algorithm moves on to the next window. If the condition is satisfied, the assessment of the spike-wave begins. To ensure uniform polarity across all signals, the signal is inverted if a minimum is detected at the framing point. Conversely, if a maximum is found, the signal remains unchanged.

After completing the framing stage, the window containing the potential spike-wave is selected and properly timed, ensuring that the maximum of derivative of the spike is positioned at the framing point (at one third of the window). This stage also allows to reduce the runtime of the algorithm, as rejected windows are not further analyzed.

2.3.1.2. Feature extraction

Fig. 2 B displays several “well-framed” spike-wave windows (top) along with their corresponding derivatives (bottom). Spike-waves, particularly during seizure onset, exhibit diverse shapes. To ensure effective spike-wave detection, an algorithm needs to be adaptable to various spike-wave shapes. Following the framing step, we extract features from both the signal and its derivative.

Fig. 2 C provides all extracted features, denoted in red (excluding SI, SID, and ZC), based on analysis of spike-wave patterns. These features are obtained from non-normalized signals and their derivatives, and listed hereafter.

- Amplitude of the signal (A)
- Amplitude of the derivative (AD)
- Amplitude of the derivative in the first half-window (AD1, samples 1 to s2) and the last two-fifths of the window (AD2, samples s3 to s)
- Length of time during which the signal remains above the minimum point value after reaching the minimum (WL, representing wave length)
- Smoothness index of the signal (SI) and its derivative (SID). The smoothness index is determined by calculating the sum of absolute increments of a signal, normalized by their respective amplitudes, at each change in direction (See Appendix)
- Length of time during which the derivative remains positive around the framing point (SL, representing spike length)
- Number of zero-crossings of the derivative in the first half of the window (ZC)

Additionally, the following features are derived from the standard deviation normalized derivative:

- Value at the framing point (DFRP), which is the point located at one third of the window

- Value at the minimum point (DMINP), which is the location of the minimum of the signal in the first half of the window
- Maximum (MAXD3) and minimum value (MIND3) of the normalized derivative in the last third of the window (samples s4 to s)

2.3.1.3. Evaluation of events of interest

Following the framing stage, some of extracted features from the current window are used to determine whether the window qualifies as an EOI. This assessment is based on a set of prerequisite conditions that must be satisfied, consisting of 11 conditions as listed in Table 1a. These conditions rely on threshold values, indicated by the bolded names in the "conditions" column, while the corresponding values of the thresholds are provided in the "values of thresholds" column. The threshold values were manually and empirically fine-tuned based on the analysis of a diverse collection of spike-wave patterns at the onset of seizures from our EEG database.

This stage is represented by the prerequisite stage box on Fig. 2 A. If all the conditions are met, the window is classified as an EOI and proceeds to the classification stage. If the conditions are not fulfilled, the window is discarded and the algorithm proceeds to the next time step.

2.3.1.4. Spike-wave classification

Once an EOI is identified, the window is forwarded to one of two types of classifier. The first classifier is a supervised deep learning model, specifically a MLP. The second classifier is an unsupervised approach based on the DTW method (classifying step box in Fig. 2 A). Details about the classifying step can be found in Table 1b.

2.3.1.4.1. Supervised method based on multilayer perceptron

The MLP takes as input 10 normalized features (listed in section 2.1.2: A, AD, SL, WL, DFRP, SI, SID, ZC, MAXD3 / DFRP and MIND3 / DFRP). It is composed of three layers with ‘relu’ activation (output size 10) and one classifying layer with ‘sigmoid’ activation. The loss function used is defined as $((1 + ytrue)(ypred – ytrue))^2$, where $ytrue$ is the label used for classification (1 for spike-wave events, 0 for non spike-wave events) and $ypred$ the output value of the MLP. This loss function was specifically designed so that the cost of spike-waves incorrectly classified as non spike-waves (false negatives) is twice the cost of non spike-waves classified as spike-waves. This ensures that the false negative rate will be minimal.

2.3.1.4.2. Unsupervised method based on dynamic time warping

DTW is an algorithm used to measure the similarity between two imperfectly synchronized signals. This method computes an optimal match between two signals where one undergoes a temporal deformation. The best path is defined as the temporal alignment which minimizes a cost function based on the Euclidean distance between one signal and all the possible deformations of the second one. Here we use a custom composite version of the standard DTW algorithm which adds to the previous minimized cost a warping cost consisting in the summation of the absolute distances between the line which fits best the points composing the matrix representation of the best path and these points themselves. Both minimized cost and warping cost are then fed to decreasing exponential functions (we used $e^{-(5x)^2}$ and $e^{-\sqrt{x}}$ respectively), and the two resulting values are multiplied to provide a similarity index value between 0 and 1, where a value of 1 denotes perfect similarity.

The DTW similarity index is computed twice, once, after z-normalization, between a template of spike-wave (Fig. 2 C) and the current EOI signal, and once, after normalization by the standard deviation, between the first derivative of the same template and the derivative of the current EOI signal. Then, from the two indices from the DWT, the maximum of both values is kept as the DTW value for that window.

2.3.1.4.3. Classifier output

During the classification process, each method produces an index ranging from 0 to 1. If this value exceeds a defined threshold (thrClassOutput1 in Table 1c), a spike-wave is detected. However, this information alone is not sufficient to detect the onset of a seizure, as the algorithm requires the detection of at least two parallel spike-waves on two channel derivations to label a seizure onset. At this point, the seizure onset detection module (Fig. 2 A, right) will take a decision based on a multiple thresholding system which will take into account the classifier output value as well as the amplitude of both the signal and the derivative of at least two detected spike-wave windows.

2.3.2. Seizure onset detection

The spike-wave detection presented in the previous chapter 2.3.1 is applied simultaneously on two channel derivations. Therefore, the positions of the spike-waves are known and can now be analyzed to detect the seizure onset. To do so, some algorithms only require quasi simultaneous detection of a single spike-wave on both channels (indicated by names containing "OS"), while others require the quasi-simultaneous detection of a succession of two spike-waves on both channels (indicated by names containing "TS"). In the latter case, the detection must occur within a specified time interval of 250-400 ms, corresponding to frequencies between 2.5 and 4 Hz. By combining different classifiers and the number of spike-waves, we have four possibilities: MLPOS, DTWOS, MLPTS, and DTWTS. The OS detection

approach allows for the early detection of a seizure since only one spike-wave is required. On the other hand, the TS approach is less prone to false detection but requires the detection of two spike-waves, resulting in a slightly delayed detection. Note that in both cases, short trains of spike-waves will be marked as seizures, which is one of the main drawbacks of focusing on early detection.

As pointed before, all classifiers produce output values between 0 and 1 (as explained in 2.3.1.4.3). If this value exceeds a threshold (referred to as "thrClassOutput1" in Table 1c), a spike-wave is detected. When either one spike-wave (in the case of OS algorithms) or two spike-waves within a specified interval (in the case of TS algorithms) are detected on both channels, a seizure onset is labeled. However, it is common to observe variability in amplitude and sharpness between the first and second spike-waves during seizure onset. To account for this variability, we have introduced double thresholding in TS algorithms. This means that one of the two spike-waves must satisfy more stringent conditions in terms of amplitude for the signal and its derivative (as specified in Table 1b), as well as conditions related to the output values of the classifiers (as specified in Table 1c). Similar variability can also occur between channels. In order to minimize occasional delays between event detections on both channels, we have implemented double thresholding for each channel. If an event is detected at high thresholds on one channel, the other channel only requires lower thresholds to trigger a seizure onset detection. To reflect this, the thresholds for the prerequisite stage have been chosen to be lower compared to subsequent thresholds for seizure detection.

Table 1b and Table 1c display the conditions for multiple thresholding as well as the values of the thresholds used for the 4 algorithms. In Table 1c, 'c' represents the output of the MLP or DTW classifiers. 'thr1' (also present in Table 1a) and 'thr2' indicate the double thresholding between channels, while 'thr' and 'thr'bis represent the double thresholding between two spike-waves on the same channel. Although we did not conduct a systematic exploration of threshold values, they were adjusted to optimize detection performance.

Refer to Supplementary Table 1 for the values of the time and standard deviation constants corresponding to the different algorithms. In the case of TS algorithms, we use two time constants, namely DMin and DRange, which define the boundaries of the time interval indicating the presence of a second spike-wave at the beginning of a seizure onset. Since we implement double thresholding for the two spike-waves, we keep in memory a maximum of two spike-waves, one inverted and one in its original form. It is important to note that for a seizure to be identified, both consecutive spikes must exhibit the same polarity (either both inverted or both not inverted). This is done to account for the fact that spike waves exhibit a similar shape during the seizure.

To facilitate this process, we use a simplified updating system. In the case that a spike-wave is detected without triggering seizure detection, if a newly detected

spike-wave has a greater value of amplitude (A), amplitude of the derivative (AD), or classifier output (c) compared to the previously detected spike-wave with the same inversion status, or if the range (detection time + DRange) of the previously detected spike-wave is less than a constant DChange, the newly detected spike-wave replaces the previously detected one as memorized spike-wave.

Regardless of the method used, once a seizure onset is detected, the detection is disabled for 10 seconds. After this period, detection is re-enabled when the standard deviation (DVar) of the signal in a defined time window falls below a defined threshold (thrVar). This ensures that the seizure onset is detected only once per seizure. Also, the 10-second period during which the detector is disabled acts as a security measure to limit the number of false alarms in case of series of close isolated spike-waves.

2.4. Comparison with a support vector machine-based algorithm

In order to compare the proposed method to classical one reported in the literature, we implemented the Support Vector Machine (SVM) classifier-based algorithm described in (Kjaer et al., 2017). This algorithm utilizes a sliding window of two seconds with a 1-second overlap (256 samples in our implementation), from which ten features are extracted : the log-sums of Daubechies 4 wavelet transform at the 32-64, 16-32, 8-16 and 2-4 Hz frequencies, the power in the 1-30 Hz band and the relative power between the 3-12 and the 1-30 Hz bands, the cross-correlations between signals in both the window and the preceding non-overlapping window, as well as between signals in the window filtered in the 3-12 and the 1-30 Hz bands respectively, the mean phase variance between the signal and the imaginary part of its Hilbert transform, and finally the variance of the Mahalanobis distance between each point of the 3-12 Hz filtered signal and the distribution of the 1-30 Hz filtered signal. Note that in our study we also adopt for algorithm a patient-nonspecific learning strategy (as for all other supervised algorithms). In addition, to optimize the effectiveness of the algorithm in our context, the version we implemented exploits quasi-simultaneous event detection on two derivations to mark a seizure. In the sequel, we named this algorithm "Kjaer256". We also adapted the Kjaer256 to our context (early onset detection), leading to modified version called "Kjaer32". To this end, the 256 sample overlap, of the two seconds window of the original method, is reduced to 32 sample overlap (1/8 second).

3. Results

The performance of the proposed algorithms was assessed on a database of 83 EEGs. More precisely, we evaluated the ability of the proposed algorithms to accurately detect, as early as possible, the onset of absence seizures for 3 different time intervals: i) large interval of 10 seconds (s), ± 5 s from the annotated onset of

the seizure, and ii) two reduced time intervals of ± 750 ms and ± 500 ms, respectively.

The quantitative evaluation of the performance of the detectors is achieved via the computation of usual classification scores, namely: i) Sensitivity (Se), i.e. the ratio between the number of true detections and the total number of labeled seizures, ii) Precision (Pr), i.e. the ratio between the number of true detections and the number of total detections, and iii) F1-score defined as: $F1_{score} = 2 \times (Pr \times Se)/(Pr + Se)$. A comparative study to two modified versions (here named Kjaer256 and Kjaer32) of a well-known detection algorithm is also provided.

In order to build our learning database for the supervised algorithms, namely those using MLP in the classification step, we launched on three additional EEGs from three patients not included in the analysis cohort an early version of our spike-wave detection algorithm (not included here), softened beforehand so as to detect not only spike-waves but also all kind of artifacts or noise events sharing a few characteristics with spike-waves. We then manually labeled all detected events into two categories: “hypothetical spike-waves” and “non-spike-waves”. This gave us 1643 events of interest, i.e. spike-waves, and 7605 events from the second category (background and other physiological and non-physiological artefacts), one third of which were randomly selected for the training in order to balance the two types of events. Then 20% of these realizations were randomly kept for the validation stage to avoid model overfitting. A similar process was used for the SVM-based algorithms of comparison, except that the same EEGs were divided into 2 s windows with 1 s of overlap to constitute the learning database for the algorithms of comparison, with windows containing at least two spike-waves labeled as seizure windows. Regarding the testing set, the 83 remaining EEGs were used to assess the performances of the studied pipelines, whether they are supervised or not: 449 seizures have been annotated and are used to test the performance of our algorithms.

3.1. Experiment 1: case of a large delay of ± 5 s from the onset

In order to assess how all proposed pipelines globally behave, we first analyze the detection rate of each of them in a large temporal interval of ± 5 s from the onset annotated by experts’ ground truth, i.e. considered as a ground truth. Every detection outside of this window being discounted as a false positive. The goal here is not to evaluate the early detection of the onset of absence seizures, but to the study the effectiveness of the proposed algorithms to accurately detect the seizures themselves. Indeed, it is easy to understand that if an algorithm is not able to detect given seizures, its ability to detect them early will also be low. Table 2 displays the Se and the Pr of the six compared pipelines. In addition, their rate of False Detections per Hour (FD/H) is also given. It can be seen that the four proposed pipelines slightly outperform the classical ones in term of Se (Se ranges from 0.93 to 0.95 for the proposed algorithms and from 0.91 to 0.92 for the classical methods). Regarding the Pr, clearly Kjaer256 and Kjaer32 (with Pr equal to 0.84 and 0.78,

respectively) are more efficient than our pipelines (with Pr range between 0.60 and 0.72). This is mainly due to the fact that we only manually labeled seizures if they present at least four consecutive spike-waves visible on most channels. Thus, because the proposed pipelines (especially DTWOS and MLPOS) are designed to early detect the onset seizures, they also detected isolated spike-waves and/or short trains of spike-waves (less than four consecutive spikes). This result can also be explained when we zoom on the FD/H, where we can effectively see the DTWOS and MLPOS exhibit the highest FD/H. In term of F1-score, illustrated in Fig. 3 B, the violin plots show that the distribution of Kjaer256, MLPTS and DTWTS present a median equal to 1, which means that all these algorithms perform perfectly on more than half of the tested EEGs. In contrast, Kjaer32, MLPOS and DTWOS perform perfectly on at least 37.5% of the 83 tested EEGs. All the previous results are also confirmed on Fig. 3 A and Fig. 3 C, where we depict, for all compared pipelines, the FD/H with a gradual drop of EEGs associated with the highest numbers of false detections, and the Se/Pr of each tested EEG, respectively. Indeed, Fig. 3 A shows that if a small number of specific EEGs are excluded from the test set (between 5 and 10 over the 83 tested EEGs), the TS pipelines reach the precision level of Kjaer32, while the OS ones tend to gradually catch up with the other pipelines. The reason is that some specific patients present a high number of isolated spike-waves or short trains of spike-waves. This can be also exhibited through the Se/Pr calculated for each EEG (Fig. 3 C), where clearly only some EEG records, such as 2, 11, 14, 32, 37, 39, 79 and 81 are associated with bad performance.

To complete our performance analysis study, Fig. 4 A illustrates the histogram of the delays of detection of all 442 seizures for each pipeline in a restricted interval of ± 2 s from the expert annotations. We can observe that MLPOS and DTWOS give us the earliest detection of the onset (most seizures are detected between 0.1 and 0.2 s after the annotated time). Then MLPOS and DTWOS offer a reasonable onset detection between 0.3 and 0.5 s, followed by Kjaer32 with most estimated onset between 0.5 and 1.2 s. Finally, Kjaer256 presents the less effective performance with a delay of detection between 0.8 and 1.8 s. Note that some seizures are detected before their ground truth onset. Typically, in these cases the onset of the seizures presents a small spike with bad SNR which is detected by the proposed methods (black arrow in Fig. 3 B), whereas the expert annotates the first spike wave with a high SNR (red line mark in Fig. 4 B).

3.2. Experiment 2: reduced delays of ± 750 ms and 500 ms from the annotated onset

Fig. 3 and 4 show how the six compared pipelines globally behave. In this section we will focus on the performance of each ones for two reduced delays of 750 ms (Table 3) and 500 ms (Table 4). Recall that the delays of 750 ms and 500 ms approximately correspond to the width of 3 and 2 consecutive spike-waves, respectively. In accordance with the overall results presented in Fig. 4, classical methods, namely

Kjaer256 and Kjaer32 completely fail to early detect the onset of absence seizures for practically all studied patients (see Fig. 5 B). Indeed, the bests Pr and Se are equal to 0.34 and 0.41, respectively, whatever the used algorithm and the studied delay. By contrast, although the MLPOS, DTWOS, MLPTS and DTWTS achieve slightly less effective performance than those obtained for a large delay of 5 s, these latter still robust especially for Se which range between 0.83 and 0.88 for MLPOS and DTWOS, and between 0.74 and 0.86 for MLPTS and DTWTS. All these remarks can also be underlined with the obtained FD/H, where clearly Kjaer 256 and Kjaer32 exhibit the highest FD/H values, followed by MLPOS and DTWOS, for both limited times delays. Interestingly, the shapes of the F1-score violin plots of the four proposed pipelines (Fig. 5 A) mimic those obtained for a large delay of 5 s (Fig. 3 B), though the distributions lose some of their unimodality, while Kjaer256 and Kjaer32 see their distribution inverted. With a restricted delay of detection of 750 ms (Fig. 5 A, left), all pipelines with the exception of the Kjaer algorithms have similar F1-Score distributions and perform perfectly on at least 37.5 % of the EEGs, with a median F1-score around 0.9. When this restricted delay is 500 ms, these pipelines all perform perfectly on one quarter of the EEGs, with MLPOS and DTWOS performing perfectly on 37.5 % of them.

3.3. Computation time and RAM usage

We provide in Table 5 the average computation time for 1 minute of signal as well as the RAM usage for the six algorithms. All the algorithms were implemented in Python on a computer equipped with an Intel® Core™ i7-1165G7 2.80 GHz processor and 16 GO of RAM DDR4. These statistics are provided for information only as the algorithms can be further optimized for real time purposes.
We see that the mean computation time for the proposed algorithms is comprised between 1.06 and 2 times the one of the reference algorithm Kjaer256 whose window's timestep is 1 s. The ratio between computation time and EEG time ranks from 0.033 for MLPOS to 0.062 for MLPTS, making any of the proposed algorithm very suitable for real time detection. RAM usage for the proposed algorithms is comprised between 0.9 and 3.2 times the RAM usage of Kjaer256. Supervised algorithms were computationally more expansive, in part due to the full loading of libraries dedicated to supervised learning.

4. Discussion

In this study, we present novel algorithms, based on characteristics of spike-wave features, meticulously designed to automatically detect the occurrence of absence seizures. Average delays of detection were as brief as 80 to 330 milliseconds following the onset depending on algorithms.

4.1. Why early detection of seizures in the context of absence epilepsy ?

Indeed, some studies suggest that it may be possible to abort absence seizures if the sensory stimulation is applied immediately after the onset (Blumenfeld, 2005) but not if the delay exceeds a few seconds after the onset (Rajna and Lona, 1989). One possible explanation is that there is a progressive involvement of the cortico-thalamo-cortical loop toward a critical threshold. Increased connections strength between the cerebral cortex and the thalamus might drive the system into ~3-Hz seizure oscillations via a supercritical Hopf bifurcation once the linear instability threshold is passed (Deeba et al., 2019). Early intervention might be able to stop the bilateral massive thalamocortical synchronization and the neuronal recruitment before the seizure steady state whereas a late intervention become ineffective. Under these conditions, an algorithm that can either predict or detect seizures early on is a prerequisite for any viable closed-loop system of seizure prevention.

4.2. Towards a spike-wave based detection strategy

A number of studies have been dedicated to the detection of SWDs, both in rodent models (Buteneers et al., 2013; Pan et al., 2007; Startceva et al., 2015; Xanthopoulos et al., 2009), and human patients (Baser et al., 2022; Dan et al., 2020; Giannakaki et al., 2019; Japaridze et al., 2022; Xanthopoulos et al., 2010; Yifei et al., 2019). Some of them can achieve remarkable performance in terms of sensitivity and precision / specificity. Nonetheless, the present study is to our knowledge the first one based on human clinical EEGs to propose algorithms especially dedicated to the detection of the onset of absence seizures and to extensively analyze their performance in terms of delays of detection. However, an early version (Duun-Henriksen et al., 2012) of the algorithm used in this study as a point of comparison to our own was reported to detect seizures with a mean delay after onset of 0.74 s and a standard deviation of 0.87 s.

From the 2000s onward, most state-of-the-art algorithms for CAE seizure detection have exploited spectral features, often based on wavelet transform or decomposition (Glaba et al., 2021; Ovchinnikov et al., 2010; Pfammatter et al., 2019; Xanthopoulos et al., 2010; Yan et al., 2022) or short time Fourier transform (Hese et al., 2023; Ozmen et al., 2021; Tsiouris et al., 2020) sometimes in combination with time-domain features (Kjaer et al., 2017; Swinnen et al., 2021). Our approach is both novel and old-school in that it only relies on time-domain features, with spike-wave detection at its core. The main reason for this is that early detection presents a different challenge compared to classical detection and, due to the thinner time resolution constraint, we decided to use a much smaller window of detection of 200 ms compared to the classically adopted 2 s fragmenter. Relying on time-domain features also enabled us to use a very small overlap while keeping the algorithm computationally fast enough for real-time detection.

Early detection was the solution we adopted, but prediction would have ideally suited our purpose. Preictal markers of SWDs have been investigated both in rodent models (Budde et al., 2022; Lüttjohann et al., 2013; Sitnikova and van Luijtelaar,

2009; Sorokin et al., 2016) and in human patients (Ouyang et al., 2013; Siegel et al., 1982), but, unfortunately, methods of prediction of SWDs based on human scalp EEG data do not appear reliable enough to this day. (Ouyang et al., 2013) used permutation entropy to discriminate between preictal, interictal and seizure periods, but significant overlap exists between preictal and interictal measures and there is no clear frontier between both types of periods. (Siegel et al., 1982) found that four of their five subjects exhibited a distinct preictal EEG pattern, but no pair of subjects exhibited a common pattern. Our decision to rely on the first spike-waves to detect seizure onsets followed a systematic assessment of the slow deviations preceding seizures visible on scalp EEGs, from which we concluded that their amplitude compared to that of interictal deviations was too variable between seizures of a same or of different patients for them to be regarded as reliable markers of seizure onsets. Other studies have been dedicated to the detection of spike-waves in a context of absence epilepsy (Quintero-Rincon et al., 2018; Quintero-Rinc'on et al., 2019), but the detectors do not seem to have been applied to seizure detection. It would be interesting to compare these spike-wave detection modules to our own. One of them is based on the same approach of similarity with a template we used for our DTW module and relies on the cross-correlation of the signal with a set of spike-wave templates.

4.3. On the performance and limits of the algorithms

We tested our algorithms on a rich clinical EEG database of 83 EEGs coming from 63 patients. Overall, false alarm detection rates appear high if we compare them with other seizure detection algorithms' performances (Naganur et al., 2022) but we have to take into consideration the fact that absence seizures have a much higher frequency of occurrence than other types of seizures like tonic-clonic seizures, and that the frequency of occurrence of an event very much determines what rate of false detection is acceptable. For instance, in (Naganur et al., 2022), 1248 tonic-clonic seizures were recorded over 66109 hours of recording, which makes roughly 0.45 seizure per 24 hours. A false alarm rate of 0.5 for 24 hours corresponds to one false alarm for one seizure, in other words a precision of 0.5. In contrast, we have an average of about 8 absence seizures per hour, equating to 192 seizures per 24 hours. With a false alarm rate of 192 for 24 hours, we would obtain the same precision of 0.5. While precision is a relative index, false alarm rates are absolute values and comparing them when the detected phenomena have different frequencies of occurrence is potentially misleading. In addition, the proposed goal was to detect not the seizure itself but its very onset, resulting in very degraded performances on a subset of our EEG database and overall inflated false detection rates. Though our algorithms are less precise than the Kjaer algorithms, they show a significant improvement in terms of delay of detection and are thus a lot more suited to our purpose of early detection. The TS algorithms detect most of the seizures with a delay of less than 500 ms after their annotated beginning. If we set the maximum delay to 750 ms, they achieve perfect performance on more than 37.5 % of EEGs. The OS algorithms detect most of the seizures with a delay of less than 200 ms, and

if we set the maximum delay to 500 ms, they also achieve perfect performance on more than 37.5 % of EEGs. It means that the OS algorithms, though potentially more prone to false detections than the TS algorithms, achieve better performance on this specific fraction of 37.5 % of EEGs.

With a maximum delay of detection of 5 s, most of our false detections were caused by isolated spike-waves or short trains of spike-waves not annotated as seizures, whose abundance explain the relatively low precision we obtain compared to other algorithms found in the literature. Nonetheless, we also have a number of spike-wave unrelated false alarms (see Fig. 6 for both types of false positives), especially with MLPOS and DTWOS. Though our algorithms seem to be resistant to movement artifacts, they were tested on clinical EEGs and subsequent tests on ambulatory device-generated EEGs would be required to assess their closed-loop viability. False negatives are rare and due to seizures with atypically shaped spike-waves. On one occasion only, because of the smoothness of the spikes on one channel, a seizure was detected by the Kjaer algorithms but by none of our TS algorithms. Inversely, a number of seizures were detected by our algorithms that went undetected by the Kjaer algorithms.

We did not investigate thoroughly and systematically the impact of the various thresholds on the performance of detection. We also noticed occasional latencies between event detections on both channels which result in delayed seizure detections. Finding a way to reduce these latencies while keeping high precision would ensure earlier detections. We made a first effort in this direction with the implementation of double thresholding for the two channels, but we believe further improvements could be introduced.

No significant difference of performance was found between our supervised (MLP) and unsupervised (DTW) algorithms. This could be due to the limited extent of our learning database which contained signals extracted from no more than three EEGs and could have been enriched in particular with “first spike-waves”, the first spike-wave of a seizure differing usually in shape from the following ones. This limitation of our study also applies to the algorithm of comparison whose learning database was constituted from the same three EEGs and could have been enriched with windows containing only two or even one spike-waves, i.e. with seizure onset windows. However, we tested such an enrichment of the learning database for the algorithm of comparison and it resulted in a significant loss in precision.

4.4. On the choice of algorithm

The choice of the adequate algorithm to be used depends primarily on the constraints we have on the suitable time of detection. This is due to the duration of the window during which an external stimulus could abort an absence seizure. A first step further could then be to systematically assess this window of opportunity, and one or several of the proposed algorithms could be an important part of the required protocol. The choice of an adequate algorithm should also depend on the profile of

the analyzed EEGs of the patient. The use of the OS algorithms, and in some cases of any of our algorithms, should in particular be excluded if the patient is prone to isolated spike-waves.

5. Conclusion

In this study, we propose a novel family of algorithms dedicated to the detection of childhood absence seizure onset. Currently, state-of-the-art algorithms for SWD detection are predominantly based on frequency domain features. We show that we can achieve equal, if not better, overall performances by relying only on time domain features, especially with respect to the timing of SWD detections. Interestingly, we also show that the unsupervised proposed methods exhibit equivalent performance comparing to the supervised ones. These algorithms are intended to be integrated into a closed-loop system, coupled with an appropriate stimulation device, designed to interfere with CAE seizures and terminate them within the shortest delays after their initiation.

All our algorithms have been tested as generic algorithms, with a patient-nonspecific strategy, and a generic template for the DTW based algorithms. They performed well on a large subset of our EEG database. A patient-specific approach with potential adjustment of some thresholds based on available EEGs might allow to achieve even better results for most patients, with the only unavoidable exception of false alarms raised by short trains of spike-waves.

Appendix

Smoothness index algorithm :

```
Output Sum = Smoothness index
    Signal2 ← Signal/(max(Signal)-min(Signal))
    Sum ← 0
    Signprec ← 0
    N ← length(Signal2)
    for i ← 1 to N-1 do
    |   if Signal2[i + 1]–Signal2[i] >= 0 then
    |   |   Sign ← 1
    |   else
    |   |   Sign ← 0
    |   end if
    |   Sum ← Sum + abs(Signal2[i + 1]–Signal2[i]) ∗ abs(Sign–Signprec)
    |   Signprec ← Sign
    end for
```

Funding

This study has been funded by the Institut des Neurosciences Cliniques de Rennes (INCR, www.incr.fr), as part of the PREDILEPSY Project.

Acknowledgement

We thank P. Van Bogaert, from the Department of Pediatric Neurology, CHU d'Angers, for revising the manuscript.

We thank Rupert Schiessl and the Predilepsy working group for their advice.

Conflict of Interest Statement

None of the authors have potential conflicts of interest to be disclosed.

References:

André-Obadia N, Parain D, Szurhaj W. Continuous EEG monitoring in adults in the intensive care unit (ICU). Clin Neurophysiol. 2015;45:39–46. https://doi.org/10.1016/j.neucli.2014.11.003.
Baser O, Yavuz M, Ugurlu K, Onat F, Demirel BU. Automatic detection of the spike-and-wave discharges in absence epilepsy for humans and rats using deep learning. Biomed Signal Process Control 2022;76:103726. https://doi.org/10.1016/j.bspc.2022.103726.
Blumenfeld H. Consciousness and epilepsy: why are patients with absence seizures absent? Prog Brain Res 2005;150:271–86. https://doi.org/10.1016/S0079-6123(05)50020-7.
Budde B, Maksimenko V, Sarink K, Seidenbecher T, van Luijtelaar G, Hahn T, et al. Seizure Prediction in Genetic Rat Models of Absence Epilepsy: Improved Performance through Multiple-Site Cortico-Thalamic Recordings Combined with Machine Learning. eNeuro 2022;9:ENEURO.0160-21.2021. https://doi.org/10.1523/ENEURO.0160-21.2021.
Buteneers P, Verstraeten D, Nieuwenhuyse BV, Stroobandt D, Raedt R, Vonck K, et al. Real-time detection of epileptic seizures in animal models using reservoir computing. Epilepsy Res 2013;103:124–34. https://doi.org/10.1016/j.eplepsyres.2012.07.013.
Crunelli V, Leresche N. Childhood absence epilepsy: Genes, channels, neurons and networks. Nat Rev Neurosci 2002;3:371–82. https://doi.org/10.1038/nrn811.
Crunelli V, Lőrincz ML, McCafferty C, Lambert RC, Leresche N, Di Giovanni G, et al. Clinical and experimental insight into pathophysiology, comorbidity and therapy of absence seizures. Brain 2020;143:2341–68. https://doi.org/10.1093/brain/awaa072.
Dan J, Vandendriessche B, Paesschen WV, Weckhuysen D, Bertrand A. Computationally-Efficient Algorithm for Real-Time Absence Seizure Detection in Wearable Electroencephalography. Int J Neural Syst 2020;30:2050035. https://doi.org/10.1142/S0129065720500355.
Deeba F, Sanz-Leon P, Robinson PA. Unified dynamics of interictal events and absence seizures. Phys Rev E 2019;100:022407. https://doi.org/10.1103/PhysRevE.100.022407.
Duun-Henriksen J, Madsen RE, Remvig LS, Thomsen CE, Sorensen HBD, Kjaer TW. Automatic detection of childhood absence epilepsy seizures: toward a monitoring device. Pediatr Neurol 2012;46:287–92. https://doi.org/10.1016/j.pediatrneurol.2012.02.018.
Fan D, Wang Q. Closed-Loop Control of Absence Seizures Inspired by Feedback Modulation of Basal Ganglia to the Corticothalamic Circuit. IEEE Trans Neural Syst Rehabil Eng 2020;28:581–90. https://doi.org/10.1109/TNSRE.2020.2969426.
Fonseca Wald ELA, Hendriksen JGM, Drenthen GS, Kuijk SMJV, Aldenkamp AP, Vles JSH, et al. Towards a Better Understanding of Cognitive Deficits in Absence Epilepsy: a Systematic Review and Meta-Analysis. Neuropsychol Rev 2019;29:421–49. https://doi.org/10.1007/s11065-019-09419-2.
Ge Y, Cao Y, Yi G, Han C, Qin Y, Wang J, et al. Robust closed-loop control of spike-and-wave discharges in a thalamocortical computational model of absence epilepsy. Sci Rep 2019;9:9093. https://doi.org/10.1038/s41598-019-45639-5.
Giannakaki K, Giannakakis G, Vorgia P, Klados M, Zervakis M. Automatic Absence Seizure Detection Evaluating Matching Pursuit Features of EEG Signals. 2019 IEEE 19th International Conference on Bioinformatics and Bioengineering (BIBE) 2019:886–9. https://doi.org/10.1109/BIBE.2019.00165.
Glaba P, Latka M, Krause MJ, Kroczka S, Kuryło M, Kaczorowska-Frontczak M, et al. Absence Seizure Detection Algorithm for Portable EEG Devices. Front Neurol 2021;12:685814. https://doi.org/10.3389/fneur.2021.685814.
Hese P, Dedeurwaerder S, Boon P, Lemahieu I, Van de Walle R. Detection of SWD in the cortical EEG of GAERS P. Van Hese, J.-P. Martens, S. Dedeurwaerdere, P. Boon, I. Lemahieu, R. Van de Walle 2023.
Japaridze G, Loeckx D, Buckinx T, Armand Larsen S, Proost R, Jansen K, et al. Automated detection of absence seizures using a wearable electroencephalographic device: a phase 3 validation study and feasibility of automated behavioral testing. Epilepsia n.d.;n/a. https://doi.org/10.1111/epi.17200.
Kjaer TW, Sorensen HBD, Groenborg S, Pedersen CR, Duun-Henriksen J. Detection of Paroxysms in Long-Term, Single-Channel EEG-Monitoring of Patients with Typical Absence Seizures. IEEE J Transl Eng Health Med 2017;5:2000108. https://doi.org/10.1109/JTEHM.2017.2649491.
van Luijtelaar G, Lüttjohann A, Makarov VV, Maksimenko VA, Koronovskii AA, Hramov AE. Methods of automated absence seizure detection, interference by stimulation, and possibilities for prediction in genetic absence models. J Neurosci Methods 2016;260:144–58. https://doi.org/10.1016/j.jneumeth.2015.07.010.
Lüttjohann A, Schoffelen J-M, van Luijtelaar G. Peri-ictal network dynamics of spike-wave discharges: phase and spectral characteristics. Exp Neurol 2013;239:235–47. https://doi.org/10.1016/j.expneurol.2012.10.021.
Maksimenko VA, van Heukelum S, Makarov VV, Kelderhuis J, Lüttjohann A, Koronovskii AA, et al. Absence Seizure Control by a Brain Computer Interface. Sci Rep 2017;7:2487. https://doi.org/10.1038/s41598-017-02626-y.
Naganur V, Sivathamboo S, Chen Z, Kusmakar S, Antonic-Baker A, O'Brien TJ, et al. Automated seizure detection with noninvasive wearable devices: A systematic review and meta-analysis. Epilepsia 2022;63:1930–41. https://doi.org/10.1111/epi.17297.
Ouyang G, Li J, Liu X, Li X. Dynamic characteristics of absence EEG recordings with multiscale permutation entropy analysis. Epilepsy Research 2013;104:246–52. https://doi.org/10.1016/j.eplepsyres.2012.11.003.

Ovchinnikov A, Lüttjohann A, Hramov A, van Luijtelaar G. An algorithm for real-time detection of spike-wave discharges in rodents. J. Neurosci. Methods 2010;194:172–8. https://doi.org/10.1016/j.jneumeth.2010.09.017.
Ozmen B, Yavuz M, Carçak N, Oglu M, Molnár Z, Onat F, et al. Automatic Detection Of Seizure Activity From EEG Recordings Of Genetic Rat Model Of Absence Epilepsy, 2021, p. 1–4. https://doi.org/10.1109/SIU53274.2021.9478005.
Pan Y, Ge SS, Tang FR, Al Mamun A. Detection of Epileptic Spike-Wave Discharges Using SVM. 2007 IEEE International Conference on Control Applications, 2007, p. 467–72. https://doi.org/10.1109/CCA.2007.4389275.
Panayiotopoulos CP. Typical absence seizures and their treatment. Archives of Disease in Childhood 1999;81:351–5. https://doi.org/10.1136/adc.81.4.351.
Pfammatter JA, Maganti RK, Jones MV. An automated, machine learning–based detection algorithm for spike-wave discharges (SWDs) in a mouse model of absence epilepsy. Epilepsia Open 2019;4:110–22. https://doi.org/10.1002/epi4.12303.
Quintero-Rincon A, Alanis M, Muro V, D'Giano C. Spike-and-Wave detection in epileptic signals using cross-correlation and decision trees. Revista Argentina de Bioingeniería 2018;22:3–6.
Quintero-Rinc'on A, Muro V, D'Giano C, Prendes J, Batatia H. A novel spike-and-wave automatic detection in EEG signals. ArXiv 2019.
Rajna P, Lona C. Sensory stimulation for inhibition of epileptic seizures. Epilepsia 1989;30:168–74. https://doi.org/10.1111/j.1528-1157.1989.tb05450.x.
Rinaldi VE, Di Cara G, Mencaroni E, Verrotti A. Therapeutic Options for Childhood Absence Epilepsy. Pediatr Rep 2021;13:658–67. https://doi.org/10.3390/pediatric13040078.
Saillet S, Charvet G, Gharbi S, Depaulis A, Guillemaud R and David O. Closed-loop control of seizures in a rat model of absence epilepsy using the BioMEA^TM; system. 2009 4th International IEEE/EMBS Conference on Neural Engineering, Antalya, Turkey: IEEE; 2009, p. 693–6. https://doi.org/10.1109/NER.2009.5109391.
Saillet S, Gharbi S, Charvet G, Deransart C, Guillemaud R, Depaulis A, et al. Neural adaptation to responsive stimulation: a comparison of auditory and deep brain stimulation in a rat model of absence epilepsy. Brain Stimul 2013;6:241–7. https://doi.org/10.1016/j.brs.2012.05.009.
Siegel A, Grady CL, Mirsky AF. Prediction of spike-wave bursts in absence epilepsy by EEG power-spectrum signals. Epilepsia 1982;23:47–60. https://doi.org/10.1111/j.1528-1157.1982.tb05052.x.
Sitnikova E, van Luijtelaar G. Electroencephalographic precursors of spike-wave discharges in a genetic rat model of absence epilepsy: Power spectrum and coherence EEG analyses. Epilepsy Res 2009;84:159–71. https://doi.org/10.1016/j.eplepsyres.2009.01.016.
Sorokin JM, Paz JT, Huguenard JR. Absence seizure susceptibility correlates with pre-ictal β oscillations. J Physiol Paris 2016;110:372–81. https://doi.org/10.1016/j.jphysparis.2017.05.004.
Startceva SA, Lüettjohann A, Sysoev IV, Van Luijtelaar G. A new method for automatic marking epileptic spike-wave discharges in local field potential signals. In: Genina EA, Derbov VL, Larin KV, Postnov DE, Tuchin VV, editors., Saratov, Russian Federation: 2015, p. 94481R. https://doi.org/10.1117/12.2179017.
Swinnen L, Chatzichristos C, Jansen K, Lagae L, Depondt C, Seynaeve L, et al. Accurate detection of typical absence seizures in adults and children using a two-channel electroencephalographic wearable behind the ears. Epilepsia 2021;62:2741–52. https://doi.org/10.1111/epi.17061.
Tsiouris KM, Konitsiotis S, Gatsios D, Koutsouris DD, Fotiadis DI. Automatic Absence Seizures Detection in EEG signals: An Unsupervised Module. 2020 42nd Annual International Conference of the IEEE Engineering in Medicine & Biology Society (EMBC), 2020, p. 532–5. https://doi.org/10.1109/EMBC44109.2020.9176082.
Wirrell EC, Camfield CS, Camfield PR, Gordon KE, Dooley JM. Long-term prognosis of typical childhood absence epilepsy: remission or progression to juvenile myoclonic epilepsy. Neurology 1996;47:912–8. https://doi.org/10.1212/wnl.47.4.912.
Xanthopoulos P, Liu CC, Zhang J, Miller ER, Nair SP, Uthman BM, et al. A robust spike and wave algorithm for detecting seizures in a genetic absence seizure model. Annual International Conference of the IEEE Engineering in Medicine and Biology-Proceedings 2009:2184–7.
Xanthopoulos P, Rebennack S, Liu C-C, Zhang J, Holmes GL, Uthman BM, et al. A Novel Wavelet Based Algorithm for Spike and Wave Detection in Absence Epilepsy. 2010 IEEE International Conference on BioInformatics and BioEngineering, 2010, p. 14–9. https://doi.org/10.1109/BIBE.2010.12.
Yan X, Yang D, Lin Z, Vucetic B. Significant Low-Dimensional Spectral-Temporal Features for Seizure Detection. IEEE Trans Neural Syst Rehabil Eng 2022;30:668–77. https://doi.org/10.1109/TNSRE.2022.3156931.
Yifei Y, Qin H, Li Y, Gao Z, Gai Z. EEG Absence Seizure Detection with Autocorrelation Function and Recurrent Neural Network, 2019, p. 3059–64. https://doi.org/10.1109/SSCI44817.2019.9002853.

Figure 1: **A.** Illustration of a typical absence seizure recorded with conventional clinical scalp EEG using a transverse montage. Seizure onset was manually annotated (blue dotted line). **B.** The same seizure with the channel derivations Fp1-T3 and Fp2-T4. The red dotted line marks an optimal instant of detection.

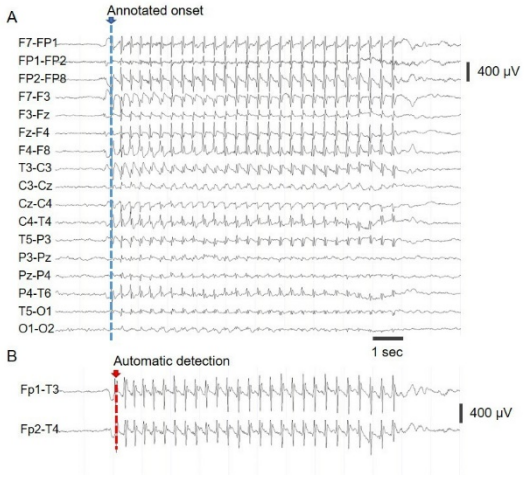

Figure 2: A. General flow charts of the algorithms. Top : an example of seizure on T3-Fp1 with two framed spike-waves (red and dotted red boxes**).** Left : flow chart of the spike-wave detection module. DTW stands for Dynamic Time Warping while MLP stands for multilayer perceptron. Right : flow chart of the seizure onset detection module. **B.** Examples of framed spike-wave shapes (top) with their derivatives (bottom). The red line marks the 0**. C.** An example of framed spike-wave with indications in red of the extracted features.

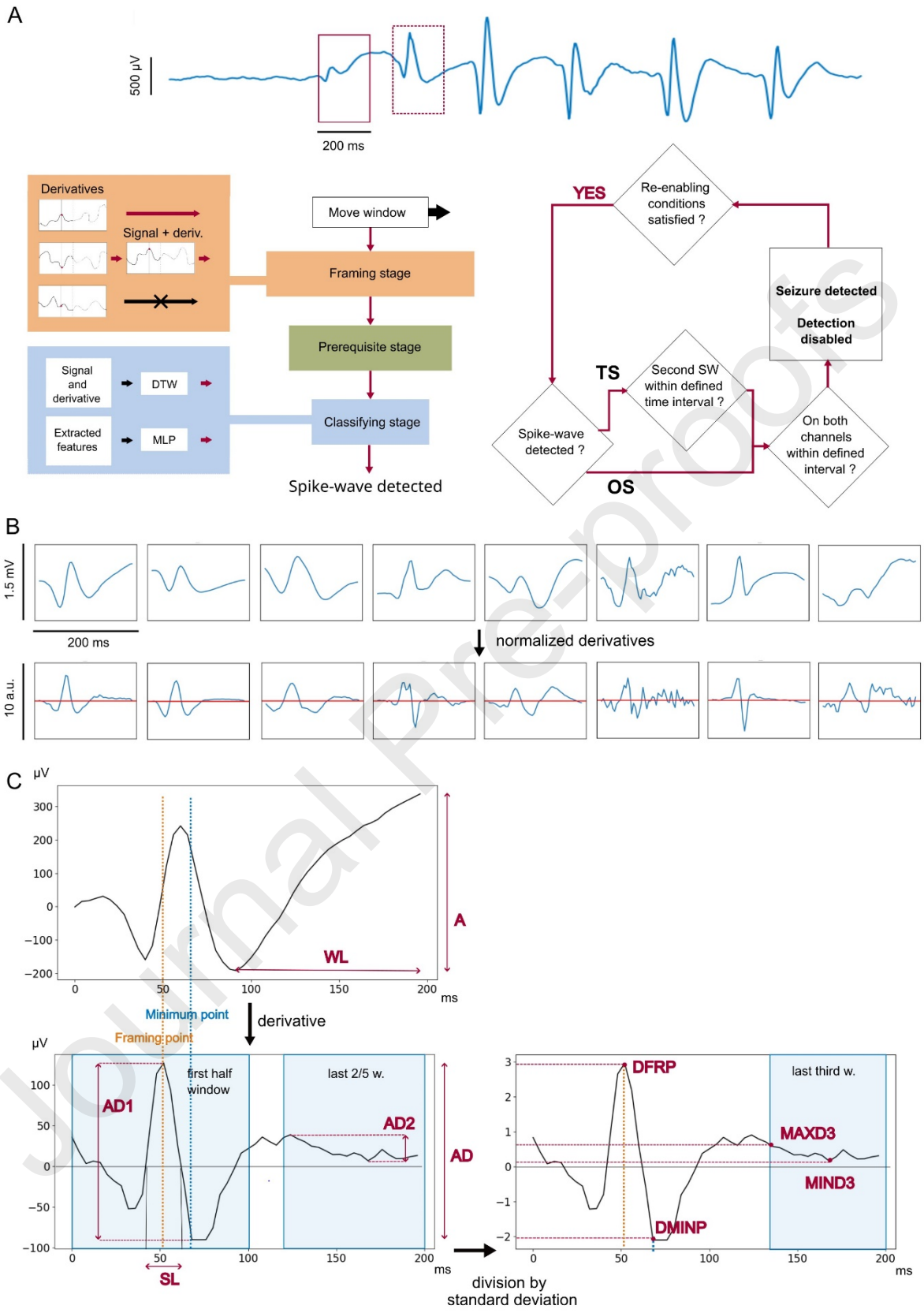

Figure 3: A. Evolution for the different algorithms of the rate of false detections per hour as we gradually drop from the statistics the EEGs associated with the highest numbers of false detections. **B.** Violin plots, for the different algorithms, of the F1-scores computed across all 83 EEGs. The * indicates the median, while the white line represents the space between the first and the third quartiles and the grey line the space between the quantiles 0.375 and 0.625. **C.** Mapping of the performance in terms of childhood (upper left corners) and precision (lower right corners) of the different algorithms for each EEG.

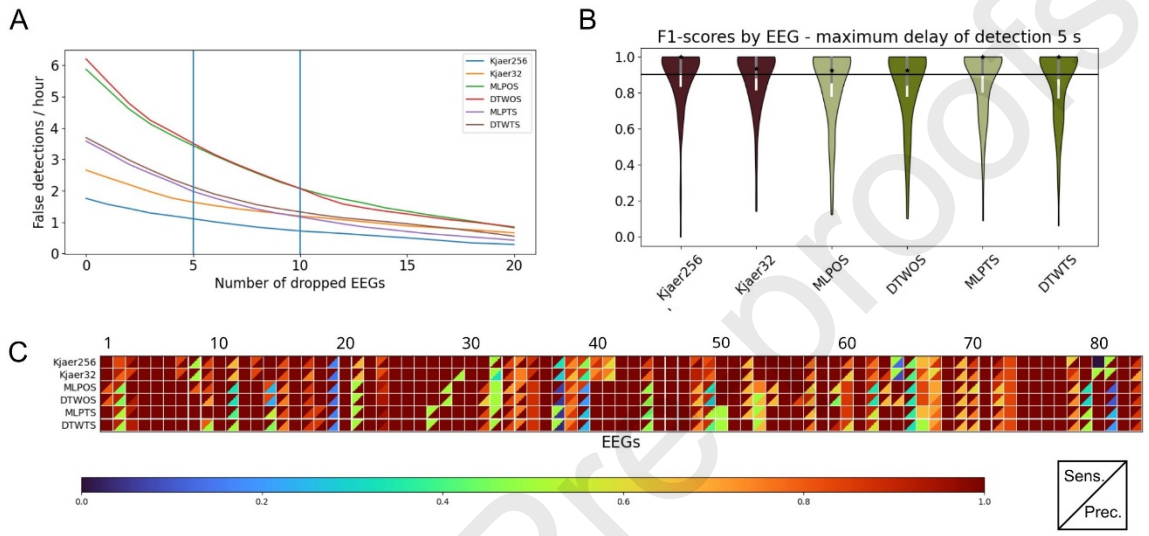

Figure 4: A. Histogram of the delays of detection of all 442 seizures in a restricted interval of ± 2 s around the annotated onsets. On top, an example of EEG signal on T3-Fp1. The red line marks the time of the annotated seizure onset. **B.** Example of EEG signal on T3-Fp1 where the seizure is detected (black arrow) before their annotated onset (red line mark).

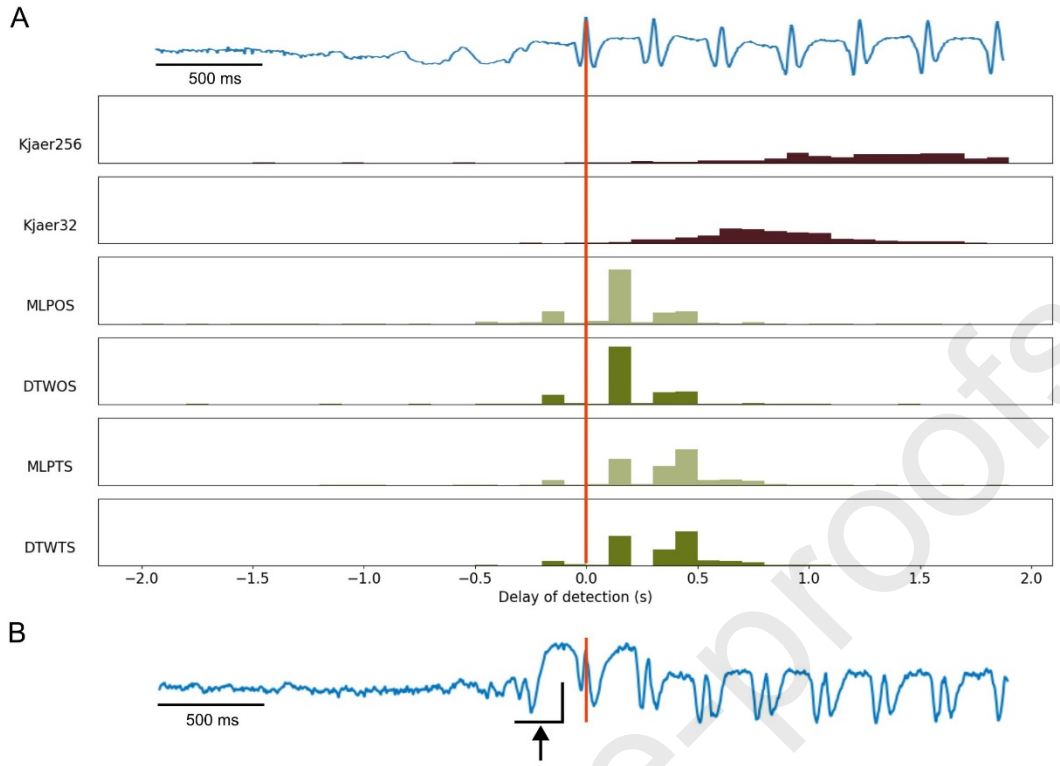

Figure 5: A. Violin plots, for different algorithms, of the F1-scores computed across all 83 EEGs, with a maximum delay of 0.75 s (left) or 0.5 s (right) between the annotated seizure onset and the time of detection for true detection. The (*) indicates the median, while the white line represents the space between the first and the third quartiles and the grey line the space between the quantiles 0.375 and 0.625. **B.** Mapping of the performance in terms of sensitivity (upper left corners) and precision (lower right corners) of the different algorithms onto each EEG, with a maximal delay of detection of 0.75 s (top) and 0.5 s (bottom).

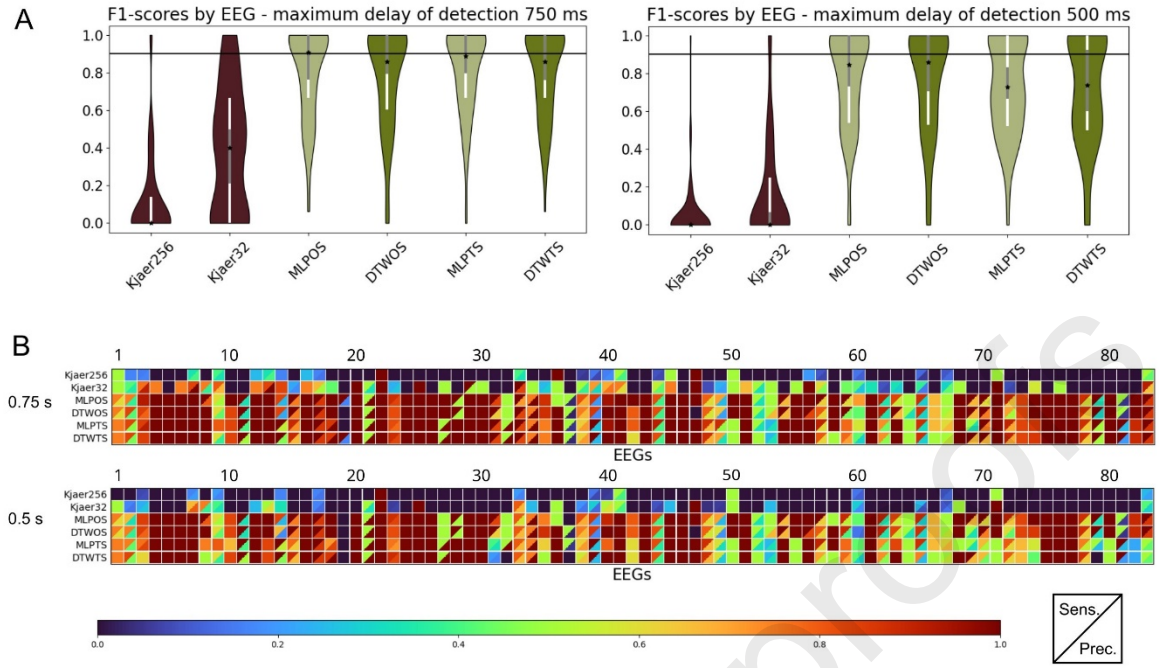

Figure 6: Examples of EEG traces associated with a false detection for one or several algorithms. In case more than one algorithm is indicated, the red lines mark the time of detection for at least one of the algorithms, while the precise time of detection for the other one(s) can precede or follow it by a few tens of milliseconds.

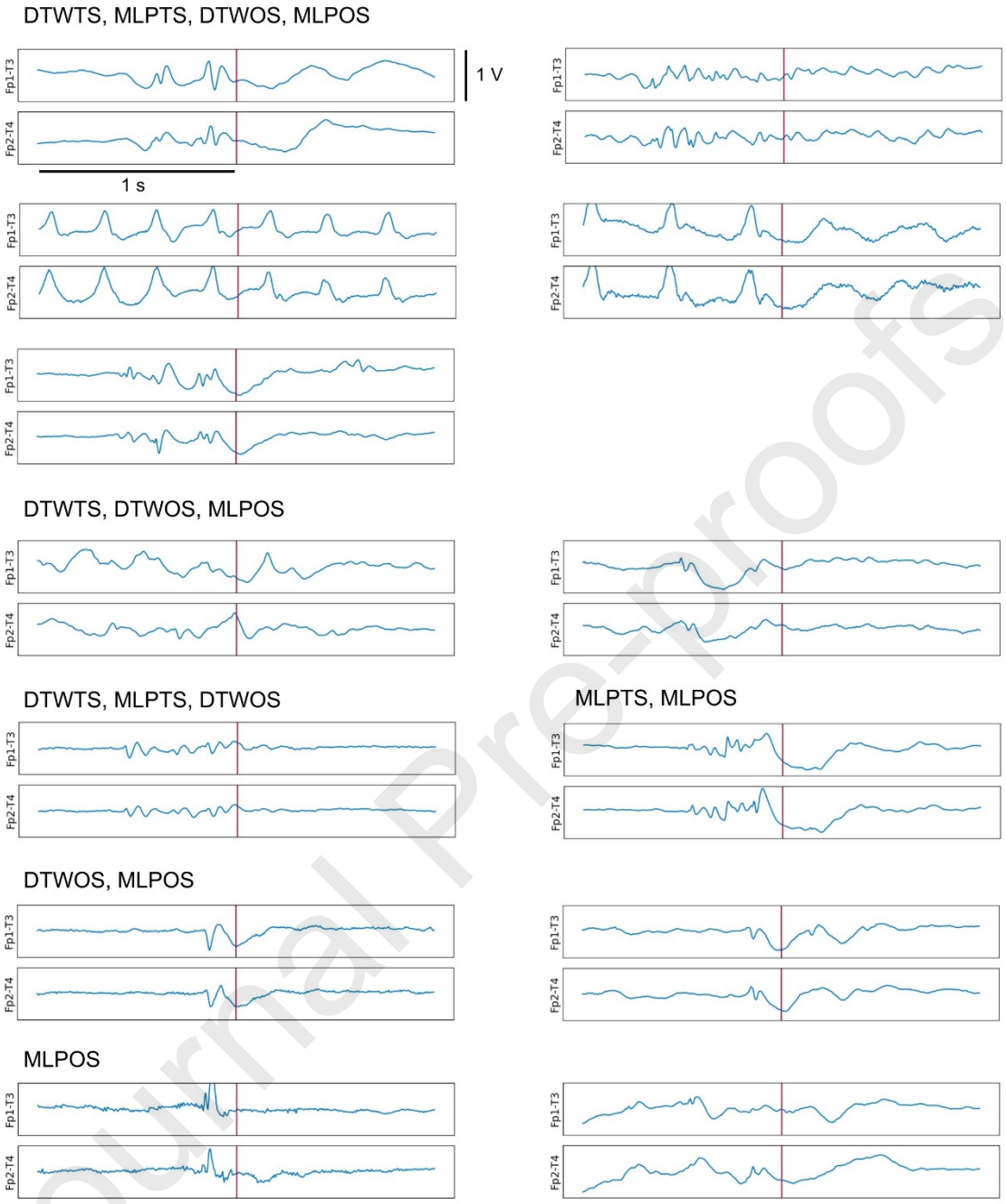

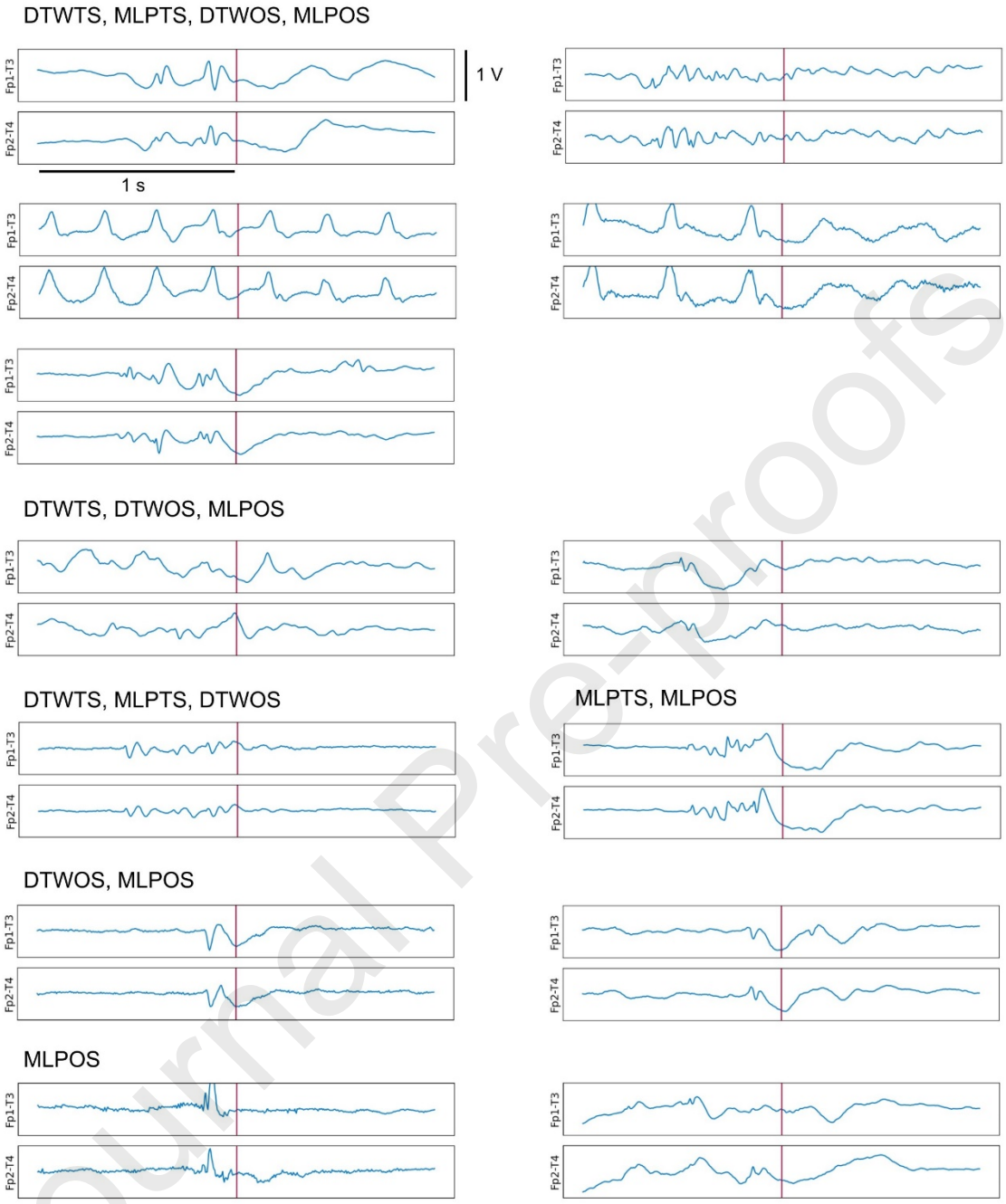

Table 1. Conditions on the extracted features for the four algorithms

1a – Prerequisite step conditions and thresholds

Conditions	**Values of thresholds**			
	MLPOS	**DTWOS**	**MLPTS**	**DTWTS**
A < **thrAmplmax**	2000			
A >= **thrAmpl1**	180		120	
AD >= **thrAmplDiff1**	70		35	

AD2 / AD1 <= **thrRatio**	0.75	1
SI <= **thrSmooth**	1.5	2
SID <= **thrSmoothDiff**	5	
ZC <= **thrHighFrequency**	10	
DFRP >= **thrMin**	0.75	
max(DFRP, abs(DMINP)) <= **thrMax**	4.5	
DMINP < **thrZero**	0	
DFRP / abs(DMINP) <= **thrRatio2**	3.5	

1b – Seizure detection step conditions and thresholds

A >= **thrAmpl1bis**		180
A >= **thrAmpl2**	225	150
A >= **thrAmpl2bis**		225
AD >= **thrAmplDiff1bis**		70
AD >= **thrAmplDiff2**	70	35
AD >= **thrAmplDiff2bis**		70

1c – Seizure detection step conditions and thresholds (classifier output)

c >= **thrClassOutput1**	0.9	0.15	0.5	0.05
c >= **thrClassOutput1bis**				
c >= **thrClassOutput2**	0.95	0.3		
c >= **thrClassOutput2bis**			0.95	0.15

Table 2. Precision, sensitivity, false detection rate and mean delay of detection, with a maximum delay of 5 s

Algorithms	Mean delay of detection	Mean precision	Mean sensitivity	Mean false detections / hour
Kjaer256	1.35	0.84	0.91	1.71
Kjaer32	0.81	0.78	0.92	2.52
MLPOS	0.08	0.62	0.95	5.83
DTWOS	0.12	0.60	0.95	6.32
MLPTS	0.33	0.72	0.94	3.67
DTWTS	0.29	0.68	0.93	4.32

Table 3. Precision, sensitivity and false detection rate, with a maximum delay of 750 ms

	Kjaer256	Kjaer32	MLPOS	DTWOS	MLPTS	DTWTS
Computation time (in s, for 1 mn of EEG)	1.86	8.82	1.98	2.28	3.72	2.94
RAM usage (in Mb)	239	242	555	246	762	215

Algorithms	Mean precision	Mean sensitivity	Mean false detections / hour
Kjaer256	0.09	0.10	9.82
Kjaer32	0.35	0.41	7.66
MLPOS	0.57	0.88	6.52
DTWOS	0.54	0.86	7.19
MLPTS	0.66	0.86	4.48
DTWTS	0.62	0.85	5.21

Table 4. Precision, sensitivity and false detection rate, with a maximum delay of 500 ms

Algorithms	Mean precision	Mean sensitivity	Mean false detections / hour
Kjaer256	0.04	0.04	10.42
Kjaer32	0.13	0.16	10.16
MLPOS	0.55	0.85	6.86
DTWOS	0.53	0.83	7.48
MLPTS	0.57	0.75	5.59
DTWTS	0.54	0.74	6.25

Table 5. Computation time and RAM usage (Hardware : processor Intel® Core™ i7-1165G7 2.80 GHz, 16 GO RAM DDR4)

Highlight

- Early detection of the onset of childhood absence seizures is mandatory to deliver an external stimulation able to inhibit them.
- An on-line process is developed to detect the onset of absence seizures from four scalp EEG electrodes.
- The proposed unsupervised solution detects most seizure onsets within a very short delay of 200 or 500 ms.